Monte Carlo Simulation of Breast Tumor Imaging Properties with Compact, Discrete Gamma Cameras[1]

G.J. Gruber, W.W. Moses, *Senior Member, IEEE,* and S.E. Derenzo, *Senior Member, IEEE*

Lawrence Berkeley National Laboratory, University of California, Berkeley, CA 94720

Abstract

We describe Monte Carlo simulation results for breast tumor imaging using a compact, discrete gamma camera. The simulations were designed to analyze and optimize camera design, particularly collimator configuration and detector pixel size. Simulated planar images of 5–15 mm diameter tumors in a phantom patient (including a breast, torso, and heart) were generated for imaging distances of 5–55 mm, pixel sizes of $2x2–4x4$ mm^2, and hexagonal and square hole collimators with sensitivites from 4000 to 16,000 counts/mCi/sec. Other factors considered included T/B (tumor-to-background tissue uptake ratio) and detector energy resolution. Image properties were quantified by computing the observed tumor fwhm (full-width at half-maximum) and S/N (sum of detected tumor events divided by the statistical noise). Results suggest that hexagonal and square hole collimators perform comparably, that higher sensitivity collimators provide higher tumor S/N with little increase in the observed tumor fwhm, that smaller pixels only slightly improve tumor fwhm and S/N, and that improved detector energy resolution has little impact on either the observed tumor fwhm or the observed tumor S/N.

I. INTRODUCTION

In recent years there has been significant interest in developing compact gamma cameras using either discrete, optically-isolated scintillator crystals with silicon photodiode readout [1–3] or pixellated cadmium-zinc-telluride (CdZnTe) solid-state detector arrays [4]. These devices present numerous advantages over traditional Anger cameras using photomultiplier tubes (PMTs) and may potentially improve nuclear medicine imaging of breast lesions and make scintimammography a valuable complement to traditional breast cancer screening techniques. Figure 1 shows the basic components of such a camera.

The performance of compact, discrete gamma cameras is strongly influenced by camera geometry, including both collimator configuration (which is critical since in single photon imaging the collimator limits both system spatial resolution and sensitivity) and pixel size. However, there has yet to be a comprehensive exploration of how camera geometry affects breast tumor imaging for these devices. Simulations to date have generally dealt with either traditional Anger cameras [5–8] or compact cameras utilizing a PSPMT (position-sensitive photomultiplier tube) [8]. Those that have analyzed discrete gamma camera geometries have looked at imaging a simple point source in the absence of background [2, 10]. The Monte Carlo code discussed in this paper was designed to be more representative of the taking of a breast
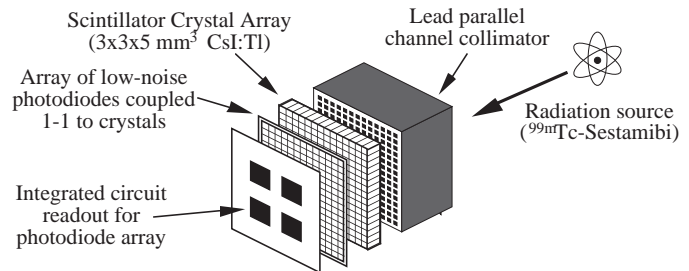

Figure 1. Basic components of a discrete gamma camera using photodiode readout of optically-isolated scintillator crystals. The scintillator crystals and photodiodes could be replaced with a pixellated CdZnTe solid-state detector array.

tumor image with a compact, discrete gamma camera and uses a 3-D phantom to study how breast lesion imaging is affected by collimator geometry, pixel size, tumor size, tumor depth, T/B uptake ratio, and detector energy resolution.

II. MONTE CARLO SIMULATION PROGRAM

The program generates gamma rays in a 3-D phantom patient (Figure 2) and determines in which camera pixel, if any, each event is detected. Moderate breast compression is assumed, hence the phantom breast thickness is 60 mm. The simulation includes both Compton scattering and photoelectric absorption within the patient. It fully implements collimator geometry—including hole diameter, hole shape (hexagonal or square), channel length, and finite septal thickness—but assumes that no photons penetrate the collimator septa and does not model either Compton scatter or x-ray fluorescence in the collimator. Detector energy resolution is included by convolving the true energy with a Gaussian whose width is proportional to the square root of the energy. Detector pixels have no spacing between them, and it is assumed that gamma rays deposit all their energy in the first pixel they encounter.
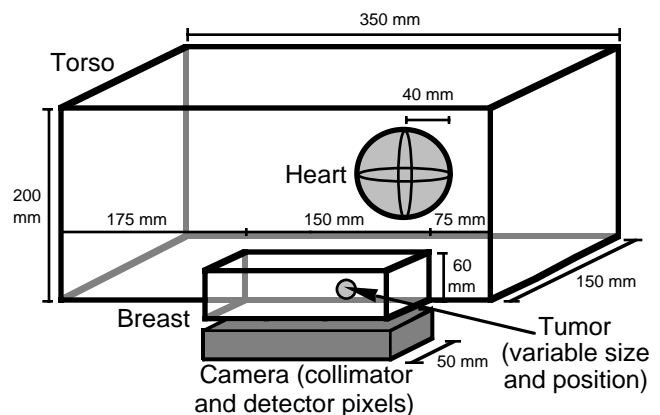

Figure 2. 3-D phantom and camera positioning used for Monte Carlo simulations designed to emulate scintimammography. The phantom includes a spherical tumor, one breast (the other is assumed shielded from the camera), a spherical heart, and a torso.

III. SIMULATION METHODS

A. Imaging Time

In order to emulate a clinical scintimammography scan the number of simulated gamma rays must be commensurate with the typical imaging time of 10 minutes. A background activity density of 80 nCi/cm^3 is assumed for the torso and breast phantom sections, while the heart activity density is assumed to be 10 times greater. Given the heart volume of 268 cm^3 and total phantom volume of 10,950 cm^3, the total phantom activity is about 1.07 mCi. This corresponds to 2.38×10^{10} gamma rays in 10 minutes, hence for each simulated scan that number of individual gammas is analyzed.

B. Photon Energy and Energy Discrimination

In all cases 140 keV gamma rays from ^{99m}Tc were simulated. Except where otherwise noted, the detector energy resolution was assumed to be 10% fwhm and the energy acceptance window 126–154 keV.

C. Generation of Background Events

The generation and scatter analysis of background events (those originating in the breast, torso, or heart) consumes the vast majority of computational time. For example, a 10 mm diameter tumor with a T/B of 10 is responsible for less than 0.04% of the simulated events. To save computational time when simulating many imaging scans under different conditions, a large number of background photons is generated and the energy, position, and direction of those photons that successfully reach the front face of the camera collimator saved. Photons randomly selected from this pool of pre-generated background gamma rays are used for breast events (~87% of the background), while algorithms mimicking the appropriate distributions are used to quickly generate torso and heart photons (~10% and ~3% of the background, respectively). Random variations in the background pattern from scan to scan are maintained, and the analysis of which photons penetrate the collimator and in which pixels they are detected is performed for all such photons during each scan. These time-saving efforts result in negligible changes to the background observed in images.

D. Characterizing Tumor Images

In order to compare tumor images from different scans, we quantify two values: observed tumor fwhm and observed tumor S/N. The tumor fwhm is calculated as the fwhm of a curve fit to the number of tumor events detected in a row of pixels. Values reported in this paper are the average of four such fwhm values for each tumor—one along each of the x, y, and two 45 degree diagonal directions. Because the fitting function requires the interpolated curve to exactly match the discrete data points, statistical variations tend to make calculated tumor fwhm values slightly smaller than the ideal for a projection image of a sphere (87% of the diameter).

Observed tumor S/N is calculated as:

$$S/N = \frac{\sum\limits_{pixels} detected\ tumor\ events}{\sqrt{\sum\limits_{pixels} all\ detected\ events}} \qquad (1)$$

where the pixels over which events are summed is adjusted to maximize the ratio. The S/N is computed using equation 1 with a symmetrical pattern of 1, 5, 9, 13, 21, 29, 37, or 45 pixels centered beneath the tumor (representing a region of interest) and the maximum value is reported. While the S/N is meant to quantify how visible a tumor would be against the background and thus allow for the comparison of images taken with different camera configurations, obviously an ROC (receiver operator characteristic) study would be necessary to quantify actual tumor detectability.

E. Expected Tumor Event Rate

Clinical scintimammography studies with traditional Anger cameras have generally shown decreased sensitivity for tumors less than 10 mm in diameter [11–12], largely due to the small volume of the tumor and hence low total activity. Table 1 displays the expected number of detected tumor-generated gamma rays for a 10 minute scan with collimators of various sensitivities and tumors of various sizes (each with a T/B of 5). Because of the count limitations inherent with imaging 5 mm tumors, we have focused our analysis on tumors 7.5 mm or larger in diameter.

Table 1.
Expected number of tumor events detected in a 10 minute scan for different collimator sensitivities and tumor sizes, assuming a T/B of 5 (activity density = 400 nCi/cm^3) and no scatter attenuation.

Collimator Sensitivity	High Resolution (4000 cps/mCi)	All Purpose (8000 cps/mCi)	High Sensitivity (16,000 cps/mCi)
	Number of Tumor Events Detected in 10 min		
5 mm tumor	63	125	250
7.5 mm tumor	210	420	850
10 mm tumor	500	1000	2000
15 mm tumor	1700	3400	6700

IV. SIMULATION RESULTS

A. Typical Tumor Images and Background Pattern

Four examples of tumor images generated by the simulation code with an optimistic T/B of 10 are presented in Figure 3, illustrating the role of tumor size and depth. A 7.5 mm diameter tumor close to the collimator (a) has a fwhm of 5.9 mm and a S/N of 17.5, while at greater depth the same tumor (b) has a similar fwhm of 6.1 mm but a S/N of only 7.5, making the tumor difficult to discern. A 15 mm diameter tumor close to the collimator (c) has a fwhm of 10.7 mm and a S/N of 62.8, while at greater depth (d) its fwhm is about the same (11.4 mm) but its S/N drops significantly to 37.2. The typical background pattern for these images has 164 counts/pixel with a standard deviation of 17.9 counts/pixel. Further, a background gradient is apparent: there are an average of 194 counts/pixel next to the chest wall and only 150 counts/pixel farthest from it.

B. Collimator Sensitivity and Hole Shape

The classic tradeoff between collimator spatial resolution and sensitivity is critical to any single photon camera. The desire to see small tumors ≤10 mm in diameter suggests emphasizing high resolution, while the count-limited situation described in Table 1 suggests emphasizing high sensitivity.
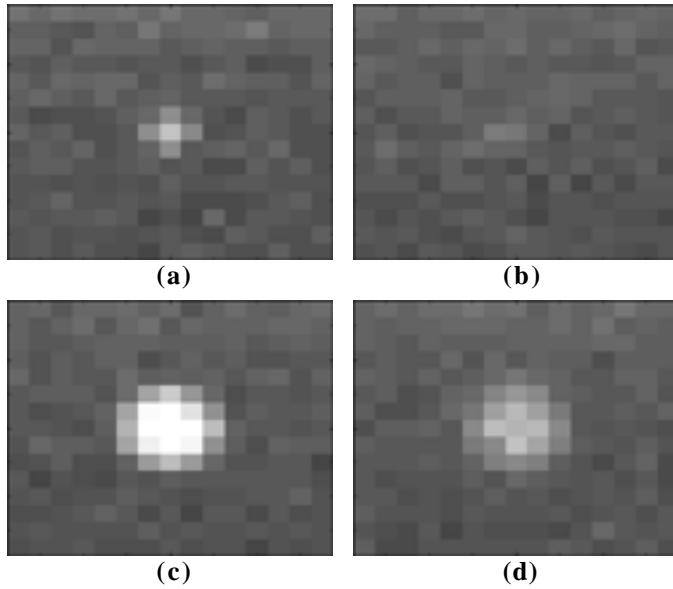
(a) **(b)**

(c) **(d)**

Figure 3: Typical images produced by the Monte Carlo simulation. A 7.5 mm diameter tumor (a) 5 mm and (b) 55 mm deep, and a 15 mm diameter tumor (c) 7.5 mm and (d) 52.5 mm deep. No grayscale enhancement or windowing has been performed. All four images use a 8000 events/mCi/sec sensitivity hexagonal hole collimator, 3x3 mm^2 pixels, and a T/B of 10. The tops of the images are closest to the chest wall.

Additionally, we must consider the possibility of using either hexagonal or square collimator holes. Hexagonal hole collimators are more readily available from industry and have a more symmetric septal penetration pattern, but square holes can be matched 1-to-1 (or even 4-to-1) to the square detector pixels and thus may provide a superior system point spread response with minimal dependence on source position by eliminating the aliasing due to geometric mismatch between hexagonal collimator holes and square detector pixels. Previous simulations suggest, however, that this aliasing problem is small for hexagonal hole collimators if the hole size is less than about half the pixel size [2].

Figure 4 displays simulation results for the observed tumor fwhm and S/N for a 10 mm diameter tumor imaged with six different collimator designs. Hexagonal hole collimators have channels 1.0 mm in diameter and 21, 15, or 10.5 mm in length, yielding sensitivities of 4000, 8000, or 16,000 counts/mCi/sec, respectively. For the square hole collimators the channels are matched 1-to-1 to the 2x2 mm^3 pixels and are 43, 31, or 22 mm in length to provide the same sensitivities, respectively, as the hexagonal hole collimators. For all configurations the septal thickness is 0.2 mm.

Little difference is evident between hexagonal and square holes, as hexagonal holes produce observed tumor fwhm and S/N values that on average are 0.1 mm greater and 2.3% smaller, respectively, than those observed when using square holes. Collimator sensitivity has only a small impact on the observed tumor fwhm—increasing the sensitivity from 4000 to 8000 counts/mCi/sec increases the observed tumor fwhm an average of 0.4 mm, and increasing the sensitivity again to 16,000 counts/mCi/sec increases the average fwhm only an additional 0.5 mm. Tumor S/N, however, is highly dependent on collimator sensitivity, as the increase from 4000 to 8000 counts/mCi/sec increases the S/N an average of 39%,
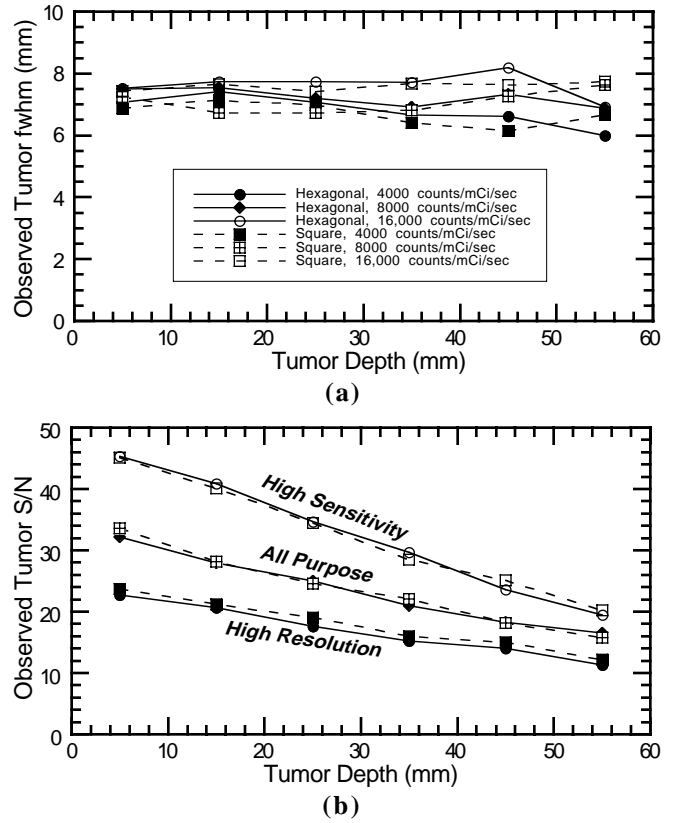

(a)

(b)

Figure 4: Dependence of (a) observed tumor fwhm and (b) observed tumor S/N on the choice of collimator. For both plots the tumor being imaged is 10 mm in diameter with a T/B of 10, while the pixel size is 2x2 mm^3.

while the increase from 8000 to 16,000 counts/mCi/sec on average increases it an additional 36%. In contrast to the typical increase in spatial resolution that occurs with greater distance from the collimator, observed tumor fwhm does not worsen significantly with increased tumor depth because the tumors are relatively close to the collimator and are large compared to the hole sizes and collimator spatial resolution. Observed S/N is strongly influenced by tumor depth (primarily due to the attenuation of tumor photons): at a depth of 55 mm the S/N averages only 48% of its value at 5 mm depth. Trends and conclusions for 7.5 mm and 15 mm diameter tumors are virtually identical.

C. Pixel Size

Smaller pixels improve the intrinsic spatial resolution and therefore can potentially improve system spatial resolution. Additionally, smaller pixel size means that the photodiodes used to read out individual scintillator crystals are also smaller, hence they will demonstrate less capacitance and dark current and thereby help improve detector energy resolution. However, decreasing pixel size does increase the density of the electronics required to read out the detector array.

Figure 5 displays simulation results for the observed tumor fwhm and S/N for different pixel and tumor sizes. Decreasing pixel size slightly decreases the tumor fwhm (more so for tumors ≤10 mm in diameter): decreasing pixel size from 4x4 mm^2 to 3x3 mm^2 results in an average fwhm decrease of 0.7 mm, while 2x2 mm^2 pixels yield a further average
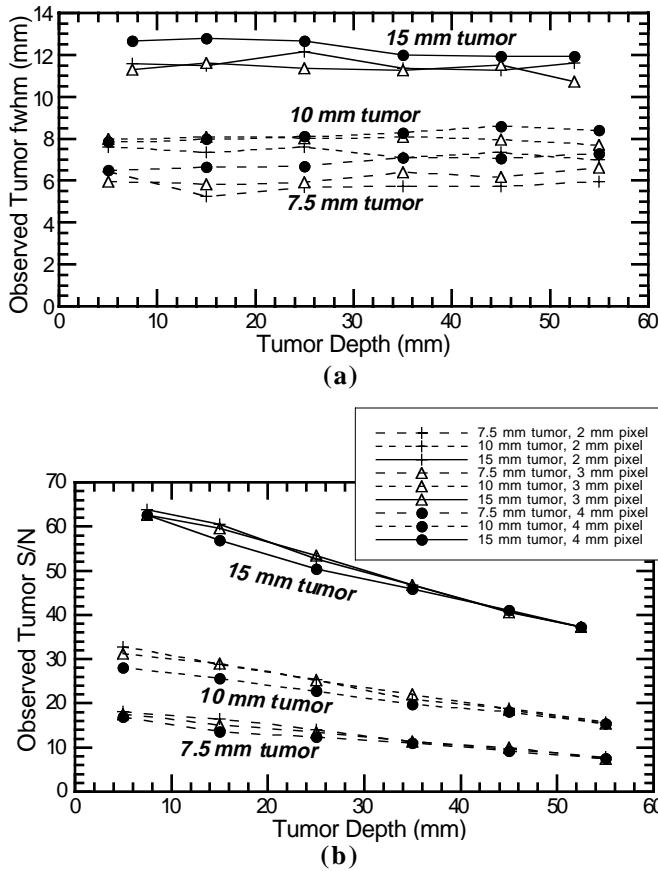
(a)

(b)

Figure 5: Dependence of (a) observed tumor fwhm and (b) observed tumor S/N on tumor diameter and detector pixel size. For both plots the collimator has hexagonal holes and a sensitivity of 8000 counts/mCi/sec, while a T/B of 10 is assumed.

decrease of 0.2 mm. Observed S/N demonstrates little dependence on pixel size—for 2x2 mm^2 pixels the S/N averages 1.2% higher than for 3x3 mm^2 pixels, which in turn averages 4.7% larger than the S/N for 4x4 mm^2 pixels. Finally, the observed S/N, as expected, depends strongly on tumor diameter: the S/N for 15 mm tumors is on average 120% larger than for 10 mm tumors, which in turn averages 85% larger than the S/N for 7.5 mm tumors.

D. Tumor-to-Background Tissue Uptake Ratio

While we have assumed a T/B of 10 for most of the simulated image acquisitions, estimates of the actual uptake ratio for breast tumors *in vivo* vary but are typically less than 10. Since the number of detected tumor events scales linearly with T/B, it is important to consider the impact that a range of T/B values will have on the acquired images.

Simulation results showing the dependence of observed tumor S/N on the uptake ratio, T/B, are given in Figure 6 for a range of tumor sizes. The observed S/N for tumors with a T/B of 10 is on average 75% larger than for tumors with a T/B of 5, which in turn demonstrate an observed S/N that averages 120% larger than for tumors with a T/B of 2. Also of note is that the 7.5 mm tumor with a T/B of 5 and both the 7.5 and the 10 mm tumors with a T/B of 2 exhibit an observed S/N of less than 10 even at a depth of only 5 mm, suggesting that smaller tumors (≤10 mm in diameter) with a low T/B (≤5) will be challenging to detect.
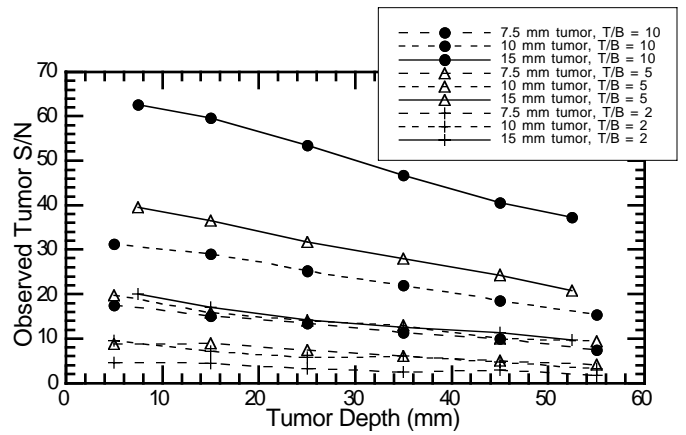

Figure 6: Dependence of observed tumor S/N on the tumor-to-background tissue uptake ratio, T/B. For all curves the collimator has hexagonal holes and a sensitivity of 8000 counts/mCi/sec, while the pixel size is 3x3 mm^3.

E. Detector Energy Resolution

Variations in detector energy resolution within the range of 5–15% fwhm have little impact on either observed tumor fwhm or S/N, as shown in Figure 7. Compared to an energy resolution of 15% fwhm, a 5% fwhm energy resolution provides an average observed tumor fwhm only 0.1 mm smaller and an average S/N only 5.2% larger. We believe this insensitivity to energy resolution is due to the low background rate at higher energies: assuming 10% fwhm energy resolution only ~20% of the image-forming photons are scattered before detection. Hence it is reasonable that under these circumstances small changes in energy resolution would not significantly affect image quality.
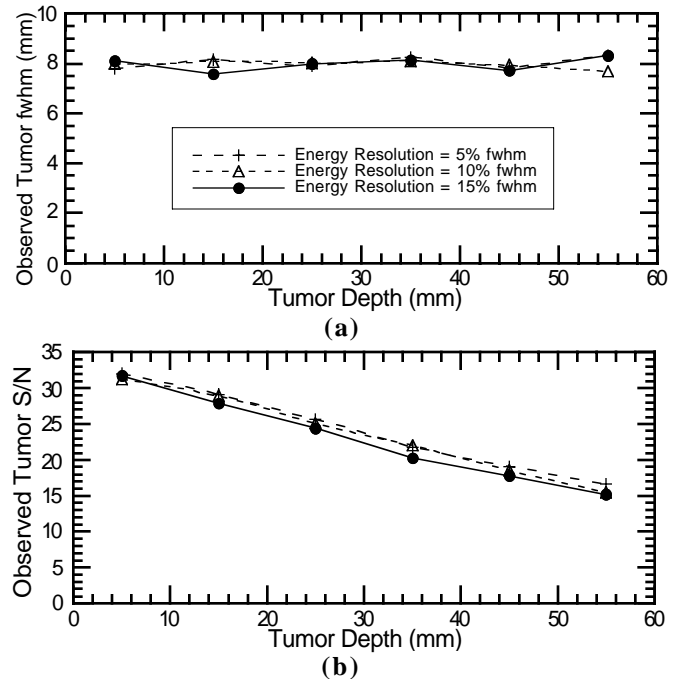

(a)

(b)

Figure 7: (a) Dependence of observed tumor fwhm and (b) observed tumor S/N on the detector energy resolution. For both plots the tumor being imaged is 10 mm in diameter with a T/B of 10, the collimator has hexagonal holes and a 8000 counts/mCi/sec sensitivity, and the pixel size is 3x3 mm^2.

V. CONCLUSIONS

In terms of observed tumor fwhm and S/N, hexagonal hole (1.0 mm diameter) collimators perform nearly as well as square hole collimators matched 1-to-1 to detector pixels. Further, hexagonal hole collimators have a more symmetric septal penetration pattern and are more readily available from industry. The geometric mismatch between hexagonal collimator holes and square detector pixels has the potential to slightly increase pixel-to-pixel variations in sensitivity, but pixel-to-pixel sensitivity variations need to be corrected through calibration regardless of the choice of collimator.

Since the tumors we expect to have enough activity to detect in 10 minutes are relatively large ($\geq$7.5 mm), tumor size tends to dominate observed tumor fwhm more than either pixel size or collimator spatial resolution. Hence the benefits of small pixels and high resolution collimators are marginal. Collimators with high sensitivities of 8000 to 16,000 counts/mCi/sec yield significantly better tumor S/N values than do high resolution collimators with 4000 counts/mCi/sec sensitivity. Further, those higher collimator sensitivities only slightly increase observed tumor fwhm. Hence, a high sensitivity hexagonal hole collimator is a wise design choice for this application.

The improved intrinsic spatial resolution offered by smaller pixels does slightly decrease tumor fwhm, especially for tumors $\leq$10 mm in diameter. Further, slight increases in observed tumor S/N are realized with smaller pixels since they are better able to conform to non-square tumor shapes. However, for both metrics the gains are small and show diminishing returns—the improvement realized by going from 3x3 to 2x2 mm^2 pixels is significantly less than realized by going from 4x4 to 3x3 mm^2 pixels. Thus, decreasing photodiode capacitance and dark current appear to be the only compelling reasons to decrease pixel size much below 3x3 mm^2, and that must be weighed against the difficulty and expense of increasing the density of the readout electronics.

Finally, variations in detector energy resolution over the range of 5–15% fwhm have very little impact on the observed tumor fwhm or S/N. This is in part due to the favorable imaging geometry assumed (Figure 2) wherein the camera does not look directly at either the heart or torso. In contrast, reference [13] suggests that energy resolution is important for scintimammography because of the prevalence of Compton-scattered events reaching the detector. However, the phantom geometry in that work was different and the range of energy resolutions examined considerably larger at 10–30% fwhm. Since 140 keV energy resolution of 8–11% fwhm has already been demonstrated with discrete scintillator/photodiode camera technology [2, 3] and 4% fwhm has been achieved with CdZnTe detector arrays [4], we feel the range of energy resolutions studied in this work is reasonable.

VI. ACKNOWLEDGMENTS

VI. REFERENCES

[1] J. Strobel, N.H. Clinthorne, and W.L. Rogers, "Design studies for a cesium iodide silicon photodiode gamma camera," *J Nucl Med*, vol. 38, pp. 31P, 1997.

[2] G.J. Gruber, W.W. Moses, S.E. Derenzo, et al., "A discrete scintillation camera module using silicon photodiode readout of CsI(Tl) crystals for breast cancer imaging," *IEEE Trans Nucl Sci,* vol. NS–45, pp. 1063–68, 1998.

[3] B.E. Patt, J.S. Iwanczyk, C. Rossington Tull, et al., "High resolution CsI(Tl)/Si-PIN detector development for breast imaging," *IEEE Trans Nucl Sci*, vol. NS-45, pp. 2126–31, 1998.

[4] J.F. Butler, C.L. Lingren, S.J. Friesenhahn, et al., "CdZnTe Solid-State Gamma Camera," *IEEE Trans Nucl Sci*, vol. NS-45, pp. 359–363, 1998.

[5] M. Ljungberg, S.E. Strand, J.E. Englund, et al., "Monte Carlo simulation of high count rate scintillation camera imaging," *IEEE NSS-MIC Conf Rec,* vol. 4, pp. 1682–86, 1994.

[6] J.S. Fleming and D.E. Simpson, "A technique for simulation of the point spread function of a gamma camera," *Phys Med Biol*, vol. 39, pp. 1457–73, 1994.

[7] J.S. Fleming, "Evaluation of a technique for simulation of gamma camera images," *Phys Med Biol,* vol. 41, pp. 1855–61, 1996.

[8] M. Spisar, J.N. Aarsvold, R.A. Mintzer, "DETECT97 simulation studies of light output in a full field-of-view small gamma camera," *IEEE NSS-MIC Conf Rec*, vol. 2, pp. 1188–92, 1997.

[9] D. Steinbach, A.R. Goode, F. Farzanpay, et al., "Development of a small-field-of-view scintimammography camera: measurements and simulations," *Proc of the SPIE—Int Soc Opt Eng*, vol. 3115, pp. 10–20, 1997.

[10] M.P. Tornai, B.E. Patt, J.S. Iwanczyk, et al., "Discrete scintillator coupled mercuric iodide photodetector arrays for breast imaging," *IEEE Trans Nucl Sci*, vol. NS–44, pp. 1127–33, 1997.

[11] H. Palmedo, A. Schomburg, F. Grunwald, et al., "Technetium-99m-MIBI scintimammography for suspicious breast lesions," *J Nucl Med*, vol. 37, pp. 626–30, 1996.

[12] F. Scopinaro, O. Schillaci, W. Ussof, et al., "A three center study on the diagnostic accuracy of ^{99m}Tc-MIBI scintimammography," *Anticancer Res*, vol. 17, pp. 1631–34, 1997.

[13] R. Pani, F. Scopinaro, R. Pellegrini, et al., "The role of Compton background and breast compression on cancer detection in scintimammography," *Anticancer Res,* vol. 17, pp. 1645–49, 1997.